Automated Microassembly using Precision based Hybrid Control

Aditya N. Das, Dan O. Popa, Harry E. Stephanou

Abstract—Microassembly is an enabling technology for micro manufacturing that offers well-known pathways to building heterogeneous microsystems with a higher degree of robustness and more complex designs than monolithic fabrication. The success of assembly in micro domain, however, is directly related to the level of precision automation employed. Control and planning are two defining factors for the microassembly yield and its cycle time. Assembly at the microscale harbors many difficult challenges due to scaling of physics, stringent tolerance budget, high precision requirements, limited work volumes, and so on. These difficulties warrant new control and planning algorithms, different than their macro-scale counterparts. In this paper, we use precision metrics to formalize a hybrid controller for automated MEMS assembly. In the past, we formulated the "high yield assembly condition (HYAC)", which gives a quantitative condition for the success and failure of compliant microassembly. Using this quatitative tool, we formalize a precision-adjusted hybrid controller switching between open, closed, and calibrated operation in the microassembly cell. Simulation and experimental results for the assembly of a microspectrometer are presented to indicate that the proposed hybrid controller lead to high yields at faster cycle times than traditional precision control methods.

I. INTRODUCTION

UNLIKE semiconductor integrated circuits (ICs), newer microsystems combine sensors, actuators, mechanical structures, electronics, and optics on a single substrate. In such a diversified system, heterogeneous manipulation of components becomes unavoidable. In an effort to find a solution for increased yields and speeds in manufacturing at the micro-scale, research initiated in 1990s has sought to understand top-down aspects of micromanipulation, sensor-based precision control of robots, self alignment effects using compliant micro structure designs, and so on.

Several papers describe and classify the architecture and algorithms used in high precision robotic cells for the purpose of directed (top-down) microscale assembly [1-4]. Multi-scale assembly methods can be classified based on throughput (serial or parallel), deliberate intervention (deterministic or stochastic), type of end-effectors (contact, non-contact) or level of human intervention (manual, teleoperated or automated). Many examples of the use of microgrippers to manipulate compliant microparts can be found, including passive grippers [5], thermal, electrostatic, or piezoelectric micro-grippers [6], or the use of adhesive forces for micromanipulation [7].

An important turning point for the practical feasibility of MEMS snap-assemblies to construct 3D microstructures occurred when Metal LIGA and Silicon DRIE (Deep Reactive Ion Etching) machining allowed for thicker 2½D part geometries. This enabled the use of automation in MEMS assembly, as pursued by several research groups [8, 9]. An example of a very well-designed fastener allowing 2½D compliant assemblies with SOI (silicon on insulator) MEMS parts is the Zyvex® connector [5].

Out-of-plane manipulation of micro-sized parts using high precision robots offers flexibility to integrate different materials, have comparatively simpler design and smaller real-estate, and use reconfigurable modular structures. However automated microassembly also requires adressing control and planning related challenges. High volume production of miniaturized devices requires the successful operation at required throughput and yield across multiple scales of tolerance, dimension and workspace limitations.

In this paper we focus on planning and control of automated deterministic serial microassembly. Typically, sequential microassembly requires a high precision micromanipulator and motion control; either by off-line programming with calibration or by on-line sensory feedback control. The latter can be accomplished via a microscope or a force sensor integrated with the gripper, or both. However, the price paid in assembly speed is considerable, resulting in low assembly throughputs. On the other hand, open loop control does not accomplish the necessary precision, but it is considerably faster and "cheaper" to implement.

A hybrid controller is proposed here, in order to take advantages of both such control methods. The tersm "hybrid" is used primarily to denote switching between feed-forward and feedback controllers based on precision metrics. The use of such control schemes is widely adopted in macro scale for a variety of control applications [10, 11], but relatively few applications use it at small scales, with the notable exceptions of vibration suppression [12]. We present preliminary experimental results for a microspectrometer, indicating that the hybrid controller achieves 35% higher accuracy than pure open loop control, while the assembly throughput is 60% faster than pure closed-loop control.

This paper is organized as follows; in section II an overview of a microspectrometer assembly problem is presented. In section III we discuss the precision metrics in microassembly scenario and the hybrid controller. Experimental results are presented in section IV along with comparative yield and cycle time of the microspectrometer assembly. Finally section V concludes the paper with

discussion of future work.

II. MICROSCALE ASSEMBLY

Manufacturing of a complex and heterogeneous microsystem involves several steps such as design, fabrication, assembly, packaging, testing etc. Whereas at the macro scales, automation is often undertaken after, and often benchmarked against manual assembly, deterministic automation at the MEMS scale requires a more holistic approach. This means that the design of the assembly cell, part and end-effectors should be considered simultaneously, and that by doing so, we can automate assembly operations in a realistic manner by ensuring higher process yield, lower cycle time and lesser sensor overhead.

A. A microassembly case study

As a case study for the proposed planner/controller, in this paper we consider the automated assembly of a *microspectrometer,* a complex MOEMS (micro-opto-electo-mechanical-systems) sensor for wide range spectrum analysis and gas detection applications [13].

A micro-robotic system called *"μ^3"* has been configured at ARRI's Texas Microfactory Laboratory to carry out general microassembly tasks (see figure 1). It consists of three robotic manipulators *(M_1, M_2 and M_3)* with 19 DoF, four high magnification microscopes to provide stereo vision for tele-operated as well as visual servoing [14].

Figure 1: μ^3 microassembly system at ARRI's Texas Microfactory.

Automated microassembly of the microspectrometer using the μ^3 poses unique challenges, because multiple heterogeneous micro-components need to be assembled with a tight mechanical, as well as optical alignment. Compliant part and socket designs are used to snap-fit several 2½D silicon MEMS parts onto the substrate. The microparts are fabricated on SOI wafers using DRIE. As seen in figure 2, automated assembly of the microspectrometer using μ^3 involves: (i) grasping of four MEMS part from the parts die using a friction-fit (or "passive" jammer) (see figure 2(b)), (ii) maneuvering the parts through collision free paths, (iii) releasing the parts onto their designated compliant sockets on the device die. Additionally two spherical lenses and one

beamsplitter cube are also aligned and assembled on the device die. Precise alignment of micro components is critical according not only to the mechanical configuration but also to the optical interference path. To ensure high yield we formulate an assemblability criterion and categorize various uncertainties that are associated with microparts and fixtures throughout the microassembly process.
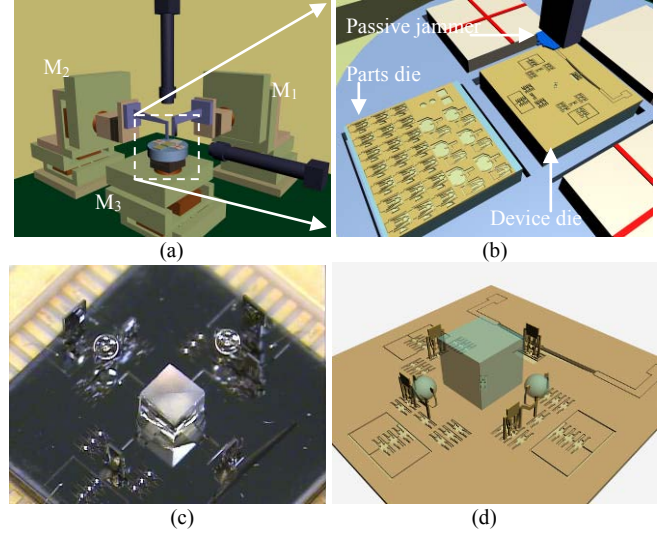

Figure 2: 3D rendering of assembly configuration of microspectrometer; (a) virtual μ^3 robotic assembly setup (b) close-up view of the micropart (mirrors, grippers, lens holders) and device dies (assembly sockets) (c) Completed microspectrometer, (d) 3D diagram of assembled 2½D MEMS parts and off-the-shelf optical components on the spectrometer substrate.

B. Assemblability criteria

Assume that a microassembly process *'P'*, carried out to assemble a specific microsystem. *'P',* can be divided into individual subtasks P_1, P_2..., P_n, where *'n'* is the number of continuous operations involving a single robot, a single part or a single tool:

$$P = \bigcup_{i=1}^{n} P_i . \tag{1}$$

Success of the designated assembly process can be represented as:

$$S(P) = \bigcap_{i=1}^{n} S(P_i), \tag{2}$$

where *'S'* is the success factor of the assembly/bonding process (a Boolean value). From equation (2) it can be inferred that the manufacturing success requires all subtasks to succeed.

In a sequential microassembly process the order of subtasks can be configured in many ways. We are interested in finding a set of ways in which the success of entire assembly is guaranteed i.e.

$$\max_{k=1 \to n!} \left(\sum_{i=1}^{n} S(P_i(O_k)) \right) = n , \tag{3}$$

where *'O_k'* is the order of subtasks in the sequence, $k = 1..n$.

If at least one solution for *'O_k'* is not found to satisfy the condition in equation (3), then the assembly will fail, and thus a change of design will be necessary, including new values for tolerances and substrate layout.

C. Categorization of microassembly task uncertainties and high yield assembly condition (HYAC)

In this paper we treat subtasks *'P_i'* as a combination of two types of positioning operations at the microscale: controllable and uncontrollable. Controllable operations *'P_i^m'* refer to spatial manipulation of components using robots. This type of manipulation will be considered to be actively controllable within certain tolerance bounds with Gaussian statistics.

On the other hand, uncontrollable operations *'P_i^b'* refer to change in component position based on the material properties, and interaction forces at the microscale. Friction based interference fitting, pneumatic grasping, surface tension, capillary stiction, adhesive bonding, etc., are some of the examples of "uncontrollable" operations. They depend on surface properties of the microparts and can act both in favor and against the assembly. We assume such operations to be uncontrollable in the sense that the assembly system may not actively correct their errors. However the effects can be predicted through appropriate models, or from experiment statistics.

Success of subtask *'Pi'* requires that the sum of the errors from *'P_i^m'* and *'P_i^b'* must be less than the design tolerance for the assembly. In this paper we assume that all errors are random Gaussian, independent distributions. This is not an unreasonable assumption in many practical instances, for example, when we combine uncertainties in fabrication, motion, sensing, and process. Moreover, in order to more easily add uniform distributions (such as tolerances) into the framework, we approximate them by a Gaussian using a 3σ spread. For instance, if we consider the design layout tolerance *'μ_{layout}'* be the result of a random Gaussian process with a 99% confidence interval, *'$3\sigma_{layout}$'*, then, for successful assembly of the subtask *'Pi'*, we must ensure that:

$$\sigma^2_{layout} > \sigma^2\left(P_i^m\right) + \sigma^2\left(P_i^b\right). \tag{4}$$

The uncertainty should also include fabrication process variances, such as patterning, photolithography, DRIE, etc, that alter the tolerance of the microparts. If we assume this error distribution to be *'$\sigma^2_{fabricaton}$'*, then the overall assembly tolerance can be represented as follows:

$$\sigma_1^2 = \left(\frac{\mu_{layout}}{3}\right)^2 + \sigma^2_{fabrication} . \tag{5}$$

In equation (5) the square term defines the assembly tolerance as a Gaussian distribution. The term μ_{layout} specifies the mean tolerance given to a specific assembly during design. In [15] we described detailed design criteria for the MEMS snap-fasteners used by the microspectrometer, including quantitative descriptions of the variance σ_1^2.

The variance due to uncontrolled operations *'$\sigma^2(P_i^b)$'* can be represented as a sum of error distributions from individual behaviors as observed from models, such as finite element analysis, or from experimenta data:

$$\sigma^2\left(P_i^b\right) = \sigma^2_{friction\_fitting} + \sigma^2_{thermal\_change} + \cdots$$
$$\sigma^2_{bonding\_shrinkage} + \cdots + \sigma^2_{material\_property} = \sigma_4^2 . \tag{6}$$

Let's now consider the controllable operations *'P_i^m'*. Assembly motion can be executed using different types of control schemes, such as:

a. Feed-forward (open loop) control, using die layout and direct robot commands without any calibration.
b. Feed-forward (open loop) control, using calibrated models of the micromanipulation robot.
c. Feedback or closed loop control, using active sensing based servoing and calibration.

For cases (a) and (b) it is necessary that the components in the assembly layout must closely match their positions in the design layout. However, in reality, the layouts do not exactly match for reasons such as tether design for fixturing the parts, fabrication uncertainties, environmental disturbances etc. Such uncertainty, assumed to be Gaussian, is denoted by its variance *'σ^2_{part}'*. In addition, the end-effector manufacturing imperfections, which are driven by fabrication errors, will have an uncertainty *'$\sigma^2_{endeffector}$'* (for instance, 2-3µm tolerances are common for the standard SOI DRIE process),. Alternatively, in case (c), where the parts and the end-effector are localized using sensors, their positional accuracy will dependent on the sensor precision. Therefore, the total part-end-effector position error distribution can be represented as follows:

$$\sigma_2^2 = \begin{cases} \sigma^2_{part} + \sigma^2_{endeffector} , open-loop \\ \sigma^2_{s\_position} + \sigma^2_{s\_measurement} , closed-loop \end{cases} . \tag{7}$$

In equation (7), *'σ_s^2'* represents sensor precision which depends on both sensor position and sensor measurement.

Next, we introduce the robot uncertainty *'σ_3^2'*, or the variance of the positional error distribution of the end-effector. Thus equation (4) can be rewritten using equations (5) - (7) as:

$$\sigma_1^2 > \sigma_2^2 + \sigma_3^2 + \sigma_4^2 . \tag{8}$$

If the errors due to uncontrollable operations are insignificant then the *'σ_4^2'* term in equation (8) can be neglected and we obtain:

$$\sigma_1^2 > \sigma_2^2 + \sigma_3^2 . \tag{9}$$

The inequality in equation (9) is defined as the "High Yield Assembly Condition (HYAC)", stating that:

"Under Gaussian uncertainty assumptions, a 99% (3σ) assembly yield can be guaranteed if the combined uncertainty of locating and positioning of microparts and end-effector is smaller than the assembly tolerance".

The HYAC is therefore a quantitative way to predict the individual success factor *'S'* of assembly. Therefore, in equation (3) *S = 1* if HYAC is true, and *S = 0* if HYAC is false for a specific assembly subtask. Furthermore, note that in the inequality for HYAC:

i. *'σ_1^2'* is "measurable" but not "correctable".
ii. *'σ_2^2'* is "measurable" and "correctable" in some cases, but this requires additional processes and resources.
iii. *'σ_3^2'* is both "measurable" and "correctable"; assuming the robot precision can be improved.

In the next sections, the goal will be to satisfy the HYAC and consequently make *S = 1*. Our controller will be chosen

such that 'σ_3^2' is minimized, depending on the complexity of the assembly task.

D. Complexity index

The complexity index (CI) of a subtask, denoted as 'Ω', and related to 'S', is a binary value used to classify an assembly subtask as high-yield or low-yield, based on associated robot and sensor precisions as well as allowed assembly tolerance budget. The idea is that a high-yield subtask is executed with faster open loop control, while a low-yield subtask is carried out with more accurate active feedback closed. Mathematically the complexity index is represented as:

$$\Omega = \frac{1-\mathrm{sgn}\left[\sigma_1^2 - \left(\sigma_2^2 + \sigma_3^2 + \sigma_4^2\right)\right]}{2} \quad (10a)$$

or

$$\Omega = \frac{1-\mathrm{sgn}\left[\left(\sigma_1^2 - \sigma_2^2 - \sigma_4^2\right) - \sigma_3^2\right]}{2}. \quad (10b)$$

From the above definition we can see that:

$$\Omega = \begin{cases} 0 \Rightarrow easy \quad to \quad assemble \\ 1 \Rightarrow hard \quad to \quad assemble \end{cases} \quad (11)$$
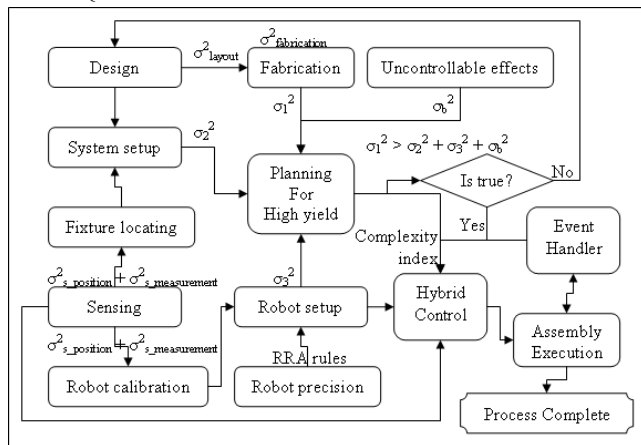

Figure 3: Process flow for microassembly automation.

Figure 3 shows a flow chart that will be used to automate the microassembly process.

III. PRECISION METRICS AND HYBRID CONTROLLER

A. Precision metrics in microassembly

Generally, the precision of a robotic system is represented by three metrics: accuracy, repeatability and resolution. We redefine these metrics to include the sensor precision which, unlike in macro-scale, is significant to the tolerance requirements of micro domain assembly. A more detailed discussion on the formulation of these definitions can be found in our previous publication [16]. The mathematical representations for the RRA (repeatability-resolution-accuracy) metrics are given below.

$$\sigma_{acc}^2 = \lim_{n \to \infty}\left[\frac{1}{n}\sum_{j=1}^{n}\left(q_j - q_{ref}\right)^2 + \frac{1}{n}\sum_{j=1}^{n}\sigma_{q_{j0}}^2\left(P_j\right)\right]+\sigma_s^2 . \quad (12)$$

$$\sigma_{rep}^2 = \lim_{n \to \infty}\left(\frac{1}{n}\sum_{j=1}^{n}\left[\left(q_j\left(P_j\right) - q_{ref}\right)\right]^2\right)+\sigma_s^2 . \quad (13)$$

$$\sigma_{res}^2 = \min\left(\lim_{\left(q_j - q_{j-1}\right)\to 0}\left[\frac{1}{n}\sum_{j=1}^{n}\left(q_j\left(P_j\right) - q_{j-1}\left(P_j\right)\right)^2\right]+\sigma_s^2\right). \quad (14)$$

In equations (12-14), 'n' is the number of measurements, '$P(j)$' is the robot path, 'q_j' is the actual joint variable, 'q_{ref}' is the desired joint value, and 'σ_s^2' is the sensor precision. Clearly, the error distribution in robot positioning is affected by the assembly sequence, choice of motion path, and precision metrics RRA:

$$\sigma^2\left(RRA\right) = f\left(P_j, \sigma_s^2\right). \quad (15)$$

B. Planning for the hybrid controller

We select the robot control among open control, feed forward control (calibration-based), and feedback control. A comparison among these schemes is shown in Table 1.

Table 1: Comparison among different control schemes

Parameters	Open loop control, No calibration	Calibration based open loop control	Closed loop control (visual servoing)
Precision attained	Low	Moderate	High
Execution time	Low	Moderate	High
Requirement	High accuracy	High repeatability	High resolution
Sensor needs	None	Minimal	Extensive
Cost of control	Low	Medium	High

A precision-adjusted hybrid controller is proposed to automate the microassembly process. Based on the RRA metrics the complexity index Ω can be calculated as $\Omega(\sigma_3^2)$ where $\sigma_3^2 \epsilon \{\sigma_{acc}^2, \sigma_{rep}^2, \sigma_{res}^2\}$, and thus Ω can be represented through either Ω_{acc}, Ω_{rep}, Ω_{res}. Table 2 shows the possible configurations of control schemes.

Table 2: Control scheme based on complexity index

Ω_{res}	Ω_{rep}	Ω_{acc}	Control Scheme
0	0	0	Open loop, no calibration
0	0	1	Open loop, with calibration
0	1	1	Closed loop, with calibration
1	1	1	Not possible with given hardware

The remaining combinations are inefficient, and hence we omitted them from table 2. The hybrid control diagram is shown in figure 4.

In this model 'u' is the desired input vector in the form of issued commands to the robot joints, and 'y' is the output vector in the form of robot poses. In this model the feedback 'K', which is the visual servoing as given by equation (19), is multiplied by the binary complexity index 'Ω' in order to select or deselect the closed loop mode. 'Ω' for a specific task is determined from the logic model, as shown in figure 4, using the RRA (resolution-repeatability-accuracy) rules given in table 2.

So the input to the system has two parts; the robot commands '$u(t)$' and the binary control loop selector '$\Omega(t)$'.

A simplified control model can be described by:

$$y[n+1] = R\left(y, \left(u[n] - \left(\Omega[n] \cdot K \cdot y(n)\right)\right)\right), \quad (16)$$

where $R(y,u)$ is the robot transfer model, u is the control input, $\Omega=0\rightarrow$open loop and $\Omega = 1\rightarrow$closed loop control.
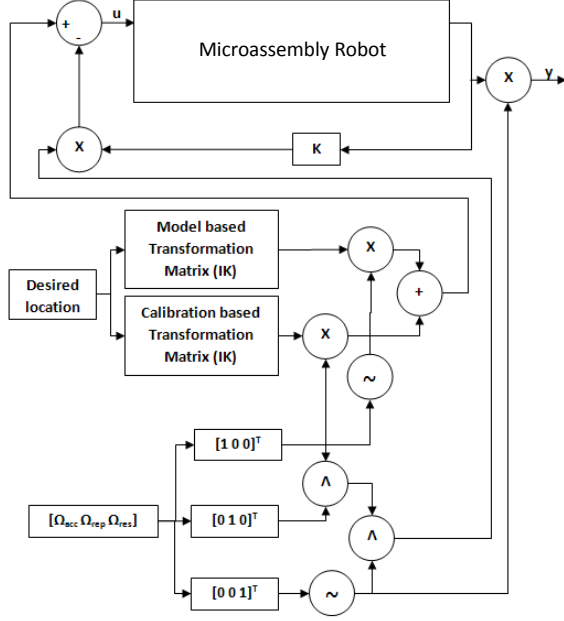

Figure 4: Plant model with the hybrid controller.

C. Open loop control – un-calibrated and calibrated

There are two cases corresponding to open loop control, un-calibrated and calibrated. In un-calibrated mode, we use the information from the MEMS die layout, and direct robot commands with nominal positional information.

In calibrated mode, we use a simple, but very effective calibration scheme based on linear interpolation of a set of taught fiducial points [14]. The calibration of our robotic cell is a one-time operation in which a die with micro features is placed on the robot and moved to a set of random locations within the sensor field (in this case, microscope cameras). The corresponding joint axis positions are noted and this data is used to relate the MEMS die coordinate system to robot coordinate system. The more calibration points we use, the better that calibration accuracy will be (bounded from below by the robot repeatability). However a large number of calibration points will make the process slower.

D. Closed loop control using active visual servoing

In closed loop control, the micro components are aligned to the desired position in the reference frame by using a Jacobian dynamic visual servoing scheme. The Image Jacobian 'J' maps the change in 2D image coordinates x, y and orientation β (measured using feature detection in Figure 5) to robot joint angles θ_1, θ_1..., θ_α where 'α' is the number of robot joints:

$$[\Delta\tilde{x} \quad \Delta\tilde{y} \quad \Delta\tilde{\beta}]^T \cong J\left[\Delta\tilde{\theta}_1 \quad \Delta\tilde{\theta}_2 \quad \cdot \quad \cdot \quad \Delta\tilde{\theta}_\alpha\right]^T. \tag{17}$$

Using the pseudo-inverse of the Jacobian matrix, we can servo the robots to desired alignment position in the sensor image coordinate frame through servoing command:

$$\left[\dot{\theta}_1 \quad \dot{\theta}_2 \quad \cdot \quad \cdot \quad \dot{\theta}_\alpha\right]^T = -cJ^+[\tilde{x} \quad \tilde{y} \quad \tilde{\beta}]^T, \tag{18}$$

where 'c' is a positive constant which acts as the gain for servoing. $\begin{bmatrix}\tilde{x} & \tilde{y} & \tilde{\beta}\end{bmatrix}^T$ gives the separation vector for the tracked feature in current sensed image data and desired image data. A PD controller is then used for the feedback control to stabilize this separation vector to zero:

$$u(t) = K_P e(t) + K_D \frac{d}{dt} e(t), \tag{19}$$

where '$e(t)$' is the tracking error given by:

$$e(t) = J^+[\tilde{x} \quad \tilde{y} \quad \tilde{\beta}]^T. \tag{20}$$

More details on how the visual servoing control is implemented can be found in [13, 16].

IV. SIMULATION AND EXPERIMENTS

A. Programming environments

Fabrication and assembly of microparts can be a time consuming and expensive process, but simulation can provide useful statistical data without experiments. In order to gather realistic simulation yield statistics, we developed a virtual 3D simulation environment called *Microsim 1.0* which allows the user to evaluate both the assembly system and task scenario. This application can test any specific assembly task for cases such as robot kinematic link misalignment, length tolerance, vibration, poor lighting conditions, etc. Once high yield assembly plans are successfully simulated, they are ported and executed on the μ^3 assembly cell via another custom built interface - *Neptune 3.0.* Both software tools were written using National Instruments® Labview® (figure 5).
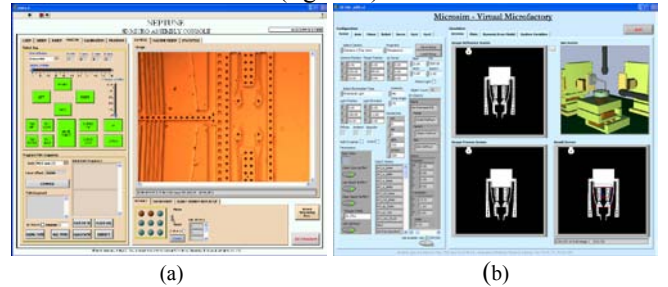

Figure 5: Snapshots of custom made applications written using Labview®
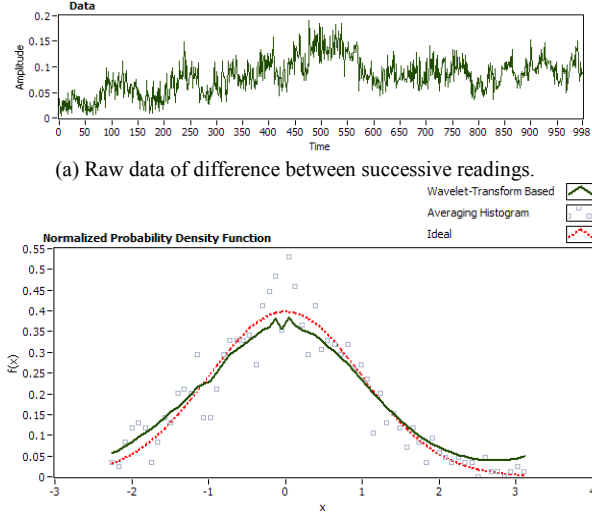(a) Neptune automation interface, (b) Microsim simulation interface.

B. Uncertainty evaluation

To check for the HYAC inequality in equation (9), we first determine the uncertainties i.e. σ_1^2, σ_2^2, σ_3^2 as well as the sensor precision σ_s^2. Actual experimental results and simulation in virtual 3D were used in conjunction to estimate the precision metrics and predict the control switching logic.

i. Sensor precision evaluation (σ_s^2)

A stationary microscope with a frame rate of 10 Hz has been used for this test. The field of view of the image captured is 1280x960 pixels at 5X magnification. For these parameters 1pixel on image corresponds to 1μm on the feature. For better resolution, sub-pixel accuracy has been used in measurements. To measure the sensor precision 1000 measurements were taken at 100ms intervals for a stationary target under the camera. The raw data was collected and the probability density function (pdf) was calculated using an

averaging histogram. A Gaussian curve is fitted to the pdf to find out the variance (figure 6).

(a) Raw data of difference between successive readings.

(b) 3σ variation estimation by Gaussian curve fitting.
Figure 6: Sensor precision evaluation.

From the above experiment, we can determine that the precision of the vision system in idle condition is 129nm along x, 124nm along y, and 20 arcsecs in θ rotation.

ii. Fabrication uncertainty and design tolerance (σ_1^2)

Chemical processes used for micromachining depend on several factors such as gas flow, exposure area, etch time and so on. For example the DRIE process generally yields an aspect ratio of 20 to 60. Thus dimensional errors in a typical DRIE micromachining process are generally less than 2 - 3 μm, while sidewall profiles are accurate within 1°.

iii. Fixturing uncertainty (σ_2^2)

To estimate σ_2^2, we conducted simulation of 1100 die placement and 1100 detethering tasks in the *Microsim 1.0* virtual 3D environment. Using the method discussed in (i) we repeatedly placed microparts in their bounding "well" fixtures to find that die placement has an accuracy of 2.4μm and a repeatability of 0.6μm. Moreover, the precision in locating a feature for part misalignment detection, turns out to have an accuracy of 0.9μm and a repeatability of 0.3μm.

iv. Robot uncertainty (σ_3^2)

After determining the precision of the vision system, we continue to estimate the precision of the robot system along individual degrees of freedom based on the path travelled by the robot. The robot used for this test case is a Cartesian robot with kinematic links configured in the order of x-translation → y-translation → θ-rotation. In this experiment, the robot is moved to several distances such as 1mm, 2mm, 5mm and 10mm etc along x, y, θ and xy directions. 250 measurement data points were collected for each case and the precision is estimated (Table 3).

From the data, it can be seen that the robot precision worsens as the distance travelled increases. Also, the precision attained along different degrees of freedom is different, even if the robot has been moved equal distances along those degrees of freedoms.

Table 3: Robot system precision test

Move case	X Precision in μm	Y Precision in μm	θ Precision in arcsec
idle	0.129	0.124	19.645
1mm x	0.444	0.166	15.637
2mm x	0.519	0.940	26.389
5mm x	0.632	1.203	33.083
1mm y	0.150	0.325	19.765
2mm y	0.280	0.455	35.709
5mm y	2.687	3.721	72.410
1mm xy	0.468	0.269	31.335
2mm xy	0.521	0.324	30.478
5mm xy	0.494	1.481	32.882

C. Hybrid controller implementation

Part 1: Offline planning based on HYAC:

Using the HYAC condition, a nominal plan for microspectrometer parts assembly was derived (table 4).

Table 4: Assembly automation sequence

Step	Operation	Control
1	Move the robots M₁, M₂, and M₃ to assembly ready positions.	calibrated open loop
2	Using active visual servoing move robot M₃ to bring the part feature to the pickup location.	calibrated closed loop
3	Bring the needle on M₁ to break the tether to release the micro part.	calibrated open loop
4	Break the tether by ramming the needle to it.	uncalibrated open loop
5	Retract the needle on M₁ back to its home position.	uncalibrated open loop
6	Using active visual servoing move robot M₃ to realign the part feature back to the pickup location.	calibrated closed loop
7	Pick up the part using the micro jammer on M₂ robot.	uncalibrated open loop
8*	Correct the error in pick up, if any, by active servoing.	calibrated closed loop
9	Move the M₃ robot to bring the socket feature into sensor field.	calibrated open loop
10	Using active visual servoing move robot M₃ to bring the socket feature to the placement location.	calibrated closed loop
11	Place the part into the socket by moving the jammer on robot M₂.	uncalibrated open loop

Part 2: Online Control Execution:

If HYAC is not satisfied prior to steps (7) & (11) respectively then we discard the subsequent steps and restart from step (1). Moreover, if the feature patterns cannot be detected due to unavailability of parts, or ambient lighting variation during steps (2), (6), (8) or (10) in the previous case then we:

   a. Go back to the previous step by reversing position.
   b. Update the uncertainty information in estimator.
   c. Re-evaluate a new path and/or control structure.
   d. Execute the new plan.

The above steps are repeated four times to complete the microspectrometer assembly. We examined the efficiency of the hybrid controller through simulation as well as experimentally. In case of simulation, we carried out 1200 simulated microspectrometer microassemblies using pure open loop control, closed loop control and proposed hybrid controller. The comparison results are given in table 5.

Table 5: Cost function comparison for 1200 simulated micro
spectrometer assemblies in virtual 3D

Parameters	Open Loop	Closed Loop	Hybrid Control
Overall yield	20%	99.9%	92.5%
Estimated time	6 to 10 min	50 to 80 min	20 to 35 min
Sensor count	0	4	2

Actual experimental implementation was carried out for 10 assemblies of microspectrometers on the μ^3 setup. As seen in Table 6, for the 10 actual assembly attempts using each of the three control structures, the hybrid controller gives 35% better accuracy than the open loop controller, while its throughput is 60% faster than a closed-loop controller. Typical value for the assembly tolerance 'σ_1^2' was 3.3µm. Almost all 10 assembly attempts failed in the open loop case, where as the hybrid control managed to achieve a higher accuracy and thus succeeded in assembling 8 out of 10 microspectrometers. Closed loop control also succeeded in assembling 9 out of 10 microsystems however it took a long time (90 minutes per system), whereas the hybrid controller managed to do the same with an average time of 40 minutes.

Table 6: Cost function comparison for 30 actual micro
spectrometer assemblies with 10 each using open loop,
closed loop and the proposed hybrid control scheme

Parameters	Open Loop	Closed Loop	Hybrid Control
Overall yield	<1%	90%	85%
Average time	6 min	90 min	40 min
Sensor count	0	4	2

V.   CONCLUSION AND FUTURE WORK

Manufacturing of microsystems can be approached either through monolithic fabrication methods or through microassembly. Although stochastic microassembly can theoretically achieve much larger throughputs within a small time in comparison to serial deterministic assembly, it is difficult to use it to construct complex, 3D devices. On the other hand, serial microassembly requires careful tuning to simultaneously achieve high assembly yield and throughput. In this paper, we proposed a precision adjusted hybrid controller in order to guarantee a high yield and improve the speed of microassembly. In contrast to conventional methods, the assembly complexity is predicted, and used to select an open or closed loop control mode based on a complexity indexΩ that depends on off -line or on-line variances related to the assembly process. Preliminary experimental results show significant improvements in assembly time with high yield guarantees.

Future work includes further characterization and refinement of the planner and controller, including formal performance guarantees,a study of tradeoffs between real-time change in tolerances, cycle time and yield, and dynamic reconfiguration of the system for other microassembly tasks.

REFERENCES

[1]   Y. Zhou, B.J. Nelson, B. Vikramaditya, *"Fusing force and vision feedback for micromanipulation"*, in Proceedings Of IEEE International Conference on Robotics and Automation, Leuven, Belgium, May 1998.

[2]   A. M. Hoover, S. Avadhanula, R. Groff, R. S. Fearing, *"A Rapidly Prototyped 2-Axis Positioning Stage for Microassembly Using Large Displacement Compliant Mechanisms"*, in Proceedings of IEEE International Conference on Robotics and Automation (ICRA), Orlando, Florida, May 2006.

[3]   D.O.Popa, H.Stephanou, *"Micro and meso scale robotic assembly"*, in SME Journal of Manufacturing Processes, Vol. 6, No.1, page(s): 52-71, 2004.

[4]   A. Rizzi, J. Gowdy, R.L. Hollis, *"Agile assembly architecture: an agent based approach to modular precision assembly systems"*, in Proceedings of IEEE International Conference on Robotics and Automation (ICRA), Vol. 2, page(s): 1511 – 1516, April 1997.

[5]   W. H. Lee, B. H. Kang, et al., *"Micropeg Manipulation with a Compliant Microgripper"*, in Proceedings of. IEEE Conference on Robotics and Automation (ICRA), Taiwan, page(s): 3213-3218, 2003.

[6]   G. Greitmann, R. A. Buser, *"Tactile microgripper for automated handling of microparts"*, Sensors and Actuators, No. 53, page(s): 410-415, 1996.

[7]   F. Arai, T. Fukuda, *"Adhesion-type micron-endeffector for micromanipulation"*, in Proceedings of IEEE International Conference on Robotics and Automation (ICRA), page(s): 1472-1477, 1997.

[8]   M. B. Cohn, K. F. Böhringer et al., *"Microassembly technologies for MEMS"*, in SPIE Micromachining and Microfabrication, Conference on Micromachining and Microfabrication Process Technology IV, Vol. 3513, page(s): 2-16, 1998.

[9]   N. Dechev, W. L. Cleghorn, J. K. Mills, *"Microassembly of 3-D microstructures using a compliant, passive microgripper"*, Journal of Microelectromechanical Systems (JMM), Vol. 13, Issue: 2, page(s): 176-189, April 2004.

[10] G. Gatti, D. Mundo, G.Danieli, *"A combined feedforward and feedback control strategy to improve the dynamic performance of cam-follower systems"*, 12th IFToMM World Congress, Besançon, France, June 2007.

[11] D. Ruiz-Vega, M. Glavic, D. Ernst, *"Transient Stability Emergency Control Combining Open-Loop and Closed-Loop Techniques"*, In Proceedings of the IEEE PES 2003 Summer Meeting. Toronto, Canada, July 2003.

[12] P. De Man, A. Preumont, *"Hybrid feedback-feedforward control for vibration suppression"*, Journal of Structural Control, Vol.3, No. 1-2, June 1996.

[13] A. N. Das, J. Sin, D. O. Popa, H. E. Stephanou, *"On the Precision Alignment and Hybrid Assembly Aspects in Manufacturing of a Microspectrometer"*, Proceedings of IEEE Conference on Automation Science and Engineering (CASE), Washington DC, USA, August 2008.

[14] A.N.Das, P.Zhang, W.H.Lee, D.O.Popa, H.E.Stephanou, *"μ^3: Multiscale, deterministic micro-nano assembly system for construction of on-wafer micro-robots"*, in Proceedings of IEEE International Conference on Robotics and Automation (ICRA), Vol. 10, No. 14, Roma, Italy, , page(s): 461–466, April 2007.

[15] R. Murthy, A.N. Das, D.O. Popa, *"High Yield Assembly of Compliant MEMS Snap Fasteners"*, Proceedings of the ASME International Design Engineering Technical Conferences & Computers and Information in Engineering Conference, Brooklyn, New York, USA, 2008.

[16] D. O. Popa, R. Murthy, A. N. Das, *"M³ - Deterministic, Multiscale, Multirobot Platform for Microsystems Packaging: Design and Quasi-Static Precision Evaluation"*, IEEE Transactions on Automation Science and Engineering (T-ASE), Vol. 6, Issue: 2, page(s): 345–361, 2008.